New Journal of Physics
The open-access journal for physics

Generation of coherent keV x-rays with intense femtosecond laser pulses

J Seres[1,6], P Wobrauschek[2], Ch Streli[2], V S Yakovlev[3], E Seres[1,4], F Krausz[1,3,5] and Ch Spielmann[4]

[1] Institut für Photonik, Technische Universität Wien, A-1040 Wien, Austria
[2] Atominstitut der Österreichischen Universtitäten, Technische Universität Wien, A-1020 Wien, Austria
[3] Department für Physik, Ludwig-Maximilians-Universität München, 85748 Garching, Germany
[4] Physikalisches Institut EP1, Universität Würzburg, 97074 Würzburg, Germany
[5] Max-Planck-Institut für Quantenoptik, 85748 Garching, Germany
E-mail: jozsef.seres@tuwien.ac.at

New Journal of Physics **8** (2006) 251
Received 14 August 2006
Published 24 October 2006
Online at http://www.njp.org/
doi:10.1088/1367-2630/8/10/251

Abstract. The realization of a compact laboratory x-ray source delivering spatially and temporally coherent ultrashort pulses is of great interest for time-resolved x-ray spectroscopy. Here, we describe the design and the parameters of a short wavelength source based on high-harmonic generation (HHG) delivering radiation up to 1.3 keV. The extension of the cutoff is attributed to intense few-cycle driving laser pulses delivered via a tabletop near-infrared laser system.

[6] Author to whom any correspondence should be addressed.

Contents

1. Introduction

A bright, coherent, pulsed laboratory x-ray source delivering keV photons will have a major impact for time-resolved x-ray spectroscopy. So far only plasma sources driven by tabletop lasers have been capable of delivering keV x-ray pulses. The emitted radiation is incoherent and the pulse duration is in the picosecond or sub-picosecond range [1]–[4]. On the other hand high-harmonic generation (HHG) in noble gases is nowadays widely used to generate spatially and temporally coherent short wavelength radiation [5, 6]. HHG can provide very short pulses having durations of a few femtoseconds down to several hundreds of attoseconds [7]–[9] as well as trains of attosecond pulses [10, 11]. However, until now, the spectral range of these laboratory x-ray sources has been limited to a few 100 eV covering e.g. the carbon K edge (284 eV) and the titanium L-edge (454 eV) [12]–[15].

In this paper, we present the design, characterization, and optimization of a HHG-based source delivering ultrashort x-ray pulses up to 1.3 keV, when driven by 5 fs laser pulses from a tabletop laser system [16]. The paper is organized as follows: in the first section, we briefly describe the laser system used for the experiments. In the next section, we discuss the set-up of the coherent x-ray source and report on their spatial and spectral characterization and its optimization. In the last section, we present computer simulations supporting the claim of generating coherent keV x-ray radiation via HHG.

2. The driving laser system

The driving laser system consists of two, cascaded, Ti:sapphire, chirped-pulse amplifiers (CPA) (figure 1) operated at a repetition rate of 1 kHz. The first amplifier stage is seeded with pulses from a commercial Ti:sapphire oscillator (Femtolasers Compact Pro, Femtolasers Produktion GmbH) having pulse duration of less than 10 fs and pulse energy of few nJ. The amplification up to the mJ level in the first stage is accompanied by strong spectral narrowing resulting in a substantial pulse lengthening. To compensate for it, we inserted an Ar-gas-filled hollow fibre between the two CPA units to nonlinearly broaden the spectrum. An acousto-optic programmable dispersive filter (DAZZLER, Fastlite) is applied for shaping the amplitude and phase of the spectrally broadened pulses resulting in nearly transform-limited pulses at the output. The spectrally broadened and shaped pulses are launched into the second CPA

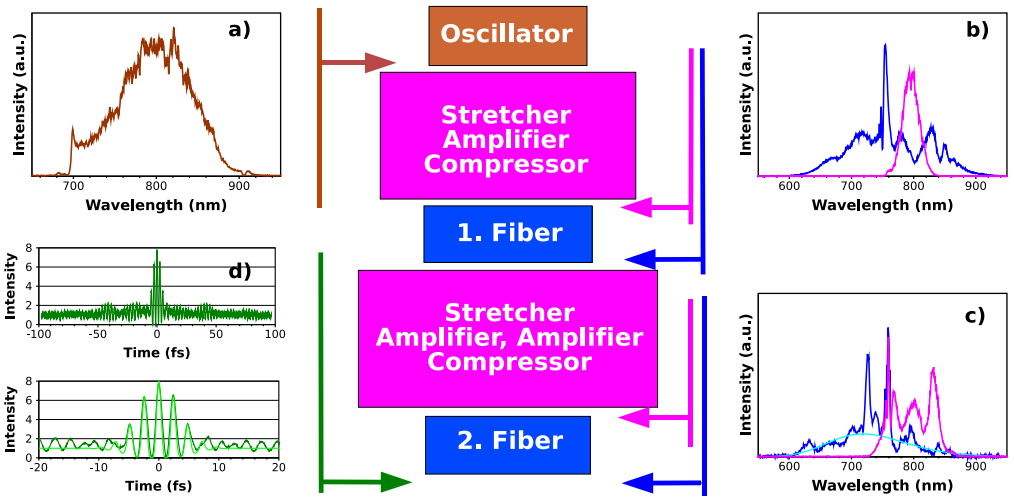

Figure 1. Building blocks of the cascaded CPA system with spectra along the chain, namely (a) after the oscillator, (b) after the first CPA (pink) and the first fibre (blue), (c) after the second CPA (pink) and the second fibre (blue). The measured autocorrelation curve of the output pulse is shown in panel (d). Also shown on an extended timescale is the measured autocorrelation in comparison with the calculated trace (light green) for 5.1 fs long Gaussian shaped pulses. Further, we have added the calculated spectrum (light blue) of a 5 fs Gaussian pulse to the measured spectra in (c) matching well the width of the measured spectra.

containing two multi-pass amplifier stages, which boost the energy up to 3 mJ. After passing a prism compressor the pulses are recompressed to ∼12 fs. A detailed description of the laser system can be found in [17]. To further shorten the pulses, they are launched into an additional 1 m-long hollow fibre with inner diameter of 0.3 mm filled with neon at 1.5 bar. After the fibre the spectrum is 160 nm broad (FWHM) and centred at 730 nm. The residual chirp is compensated by multiple reflections off specially designed ultra-broadband chirped-mirrors. At the end of the system, the linearly polarized 1 mJ laser pulses are as short as 5 fs. The pulse duration has been estimated from an autocorrelation measurement assuming a Gaussian pulse shape. The above-mentioned spectra and autocorrelation of the output pulses are shown in figure 1.

3. The high-harmonic source

The output beam of the amplifier was focused into a He gas jet (figure 2), using a spherical mirror with a focal length of 150 mm. The gas jet was continuously backed with helium at pressure in the order of one bar. From the pulse parameters (1 mJ, 5 fs) and spot size ($30 \pm 5\mu$m beam waist), we estimated the on-axis peak intensity to $\sim 1.4 \times 10^{16}\,\mathrm{Wcm}^{-2}$. The maximum x-ray photon energy $E_{\max}$ for single atom emission is given by $E_{\max} = W_b + 3.2\,U_p$, where W_b and U_p are the ionization potential of the used noble gas and the ponderomotive potential of the optical field, respectively. For the intensity realized in the current experiment the estimated cutoff is approximately 2.5 keV. HHG is a coherent process thus the number of generated photons depends on the coherence length. Unfortunately, for very high harmonics the coherence length becomes very short, dramatically reducing the flux of high-energy photons. In a recent experiment, we

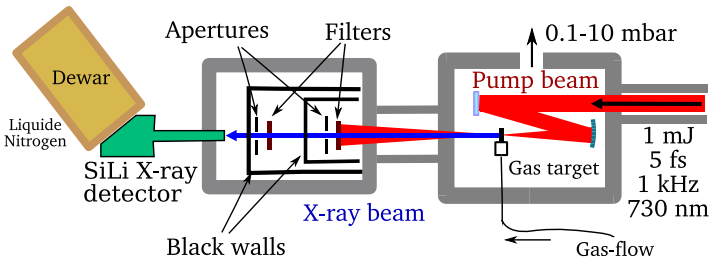

Figure 2. Set-up for the HHG source with He gas jet and for measurement of the generated x-ray after filters and apertures with liquid nitrogen cooled semiconductor detector.

have shown that non-adiabatic self-phase matching (NSPM) leads to a substantial increase of the coherence length. According to theory [18], it is necessary to use sub-10 fs pulses at intensities well above 10^{15} Wcm^{-2} to exploit NSPM. Both requirements are well met in our current experiment.

The high-harmonic pulses were detected and analysed by an energy-dispersive x-ray spectrometer. It consists of a liquid-nitrogen-cooled, semiconductor detector (Oxford, SiLi) and a multi-channel pulse-height analyser read out by a computer. The spectrometer works in the single photon detection mode, thus it must be ensured that not more than one photon per x-ray pulse hits the detector. To this end, filters and apertures were inserted into the beam to suppress the fundamental laser light and to reduce the x-ray photon number to an appropriate level for the detector. Beside the input window of the detector containing mainly aluminium and carbon, an additional 100 nm thick aluminium foil in front of the detector has been used in all experiments. To calibrate the spectrometer and measure the photon flux in different energy ranges, we inserted also thin carbon, titanium and copper filters. For all filter combinations, only photons with energies above ∼200 eV reached the detector.

3.1. Spectral characterization

The measured spectra after insertion of different filters together with the calculated filter transmission are summarized in figure 3. In all measurements, we could reproducibly detect photons up to ∼1.3 keV. The carbon, titanium and copper filters are 170, 200 and 100 nm thick, respectively. The K-edge of carbon at 280 eV and the L-edges of titanium at 454 eV and copper at 952 eV are clearly visible in the corresponding spectrum. To obtain reliable data, we attenuated the signal reducing the count rate in accordance with Poisson statistics. For the three spectra the count rates were 0.15, 0.17 and 0.33 photons pulse^{-1}, respectively. To obtain a good signal to noise ratio the total integration time for the three spectra was 100, 1000 and 1000 s, respectively.

Taking into account the attenuation of the apertures, x-ray filters, and detector window and the sensitivity of the EDX detector, we can estimate that 10^2–10^3 photons s^{-1} are generated at 1 keV in 10% bandwidth. This corresponds to a conversion efficiency of 10^{-15} from the fundamental beam into a single harmonic line in this spectral range.

3.2. Propagation properties of the x-ray beam

Among the laser generated x-ray sources, HHG radiation has an additional unique feature namely the spatial coherence. To prove that HHG is the relevant generating process in our experiment

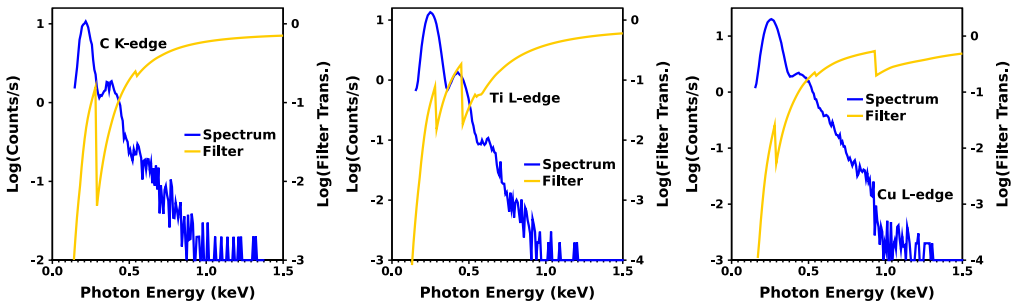

Figure 3. Photon energy spectra (blue) of coherent soft-x-ray emission from He gas driven by 5 fs, 1 mJ pulses of a table-top Ti:sapphire amplifier system inserting carbon, titanium and copper thin film filters (yellow) into the x-ray beam, respectively.

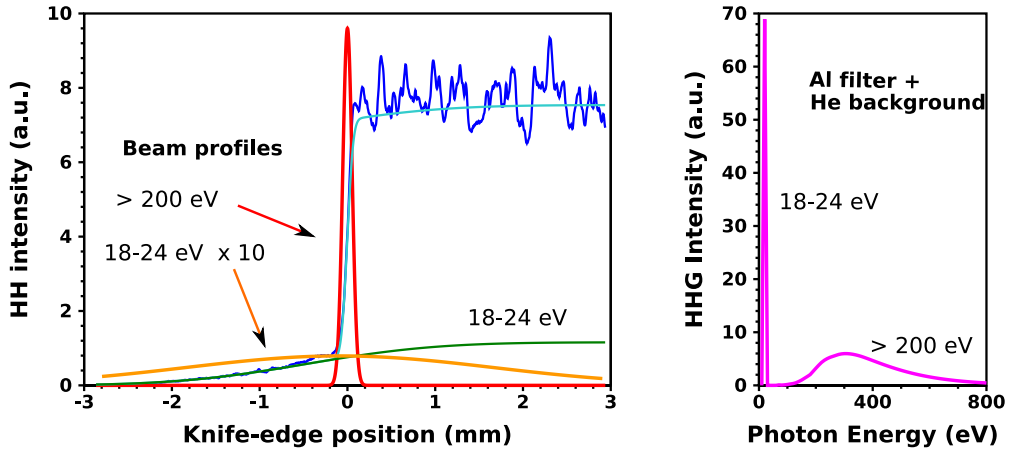

Figure 4. Measured HHG signal (blue) from the knife-edge measurement as the knife-edge moved across the HHG beam and the fitted curve (light blue) assuming a sum of two Gaussian shape beams (red and yellow) with different divergences. The contribution of the larger diameter beam to the measured signal is also plotted (green). The right figure shows the calculated spectrum transmitted through 100 nm Al.

we spatially characterized the emitted radiation. The spatial properties of the x-ray beam were examined by measuring the spectrally integrated x-ray intensities, while scanning a knife-edge across the x-ray beam. The knife-edge was placed 60 cm downstream from the helium gas jet and scanned with a calibrated linear motor. For this experiment, we replaced the EDX detector with a photo-multiplier (Channeltron 4715G, Kore Technology). For this measurement, we put also an additional 100 nm aluminium filter into beam path to filter out a fraction of generated x-ray spectra. If we assume the generated x-ray flux exponentially decays with the photon energy, which is reasonable according to the measured spectra (figure 3), the detected spectrum contains two well-separated spectral parts, one between 18 and 24 eV and another above 200 eV (figure 4). The spectrally and spatially integrated signal as a function of the knife-edge position is shown in figure 4. To the measured signal, we fitted the sum of two integrated Gaussian distributions.

The best fit was obtained for two beams having a divergence of 4.5 and 0.2 mrad (figure 4), respectively.

In a second step, we have to assign the two beams to the two different photon energy ranges. To identify the wavelength, we evaluated the photon statistics before and after the nominal knife-edge position zero. We have measured the signal I and the mean amplitude fluctuation ΔI of the signal at the two positions. For negative positions, we took only the measured signal; for positive delays we subtracted the slowly varying part of the signal. The measured signal is proportional to the photon number N, the photon energy E_{phot}, and a factor α accounting for the sensitivity of the detector at a certain photon energy. For the photo-multiplier used in our experiment, the quantum efficiency is nearly constant ($\sim$10%) in the VUV and soft x-ray range. Furthermore the fluctuations of the x-ray signal ΔI are directly proportional to ΔN. To infer photon energy from the measurements, we took advantage of the fact that for the Poisson distribution the standard deviation of the photon number ΔN is equal to the square root of the mean value $\langle N\rangle$. Assuming Poisson statistics, we can express ΔI also as a product of the square root of the mean value $\langle N\rangle$ and a numerical proportionality factor β. With this assumption, we can calculate the photon number from the measured signal and the fluctuation:

$$I = \alpha E_{\text{phot}}\langle N\rangle, \quad \Delta I \propto \Delta N = \beta E_{\text{phot}}\sqrt{\langle N\rangle}, \quad \Rightarrow \langle N\rangle = \left(\frac{\alpha}{\beta}\right)^2 \left(\frac{I}{\Delta I}\right)^2. \tag{1}$$

By comparing the ratio of the intensity to the photon number measured for the two different positions we can estimate the ratio of the photon energies dominating the signal properties.

$$\frac{\langle I_2\rangle}{\langle N_2\rangle}\frac{\langle N_1\rangle}{\langle I_1\rangle} = \frac{E_{\text{phot},2}}{E_{\text{phot},1}}. \tag{2}$$

With the measured intensities and fluctuation before (position 1) and after (position 2) the centre the ratio has been approximated to be 12. In the spectrum (figure 4), we see two clearly distinguishable photon energy ranges with their centre of gravity at 21 and 250 eV. Assuming the signal for negative positions stems from the low energy photons and the signal for positive positions is dominated by high energy photons, we find the same ratio as for equation (2). The evaluation of the position-dependent photon statistics unambiguously proves that the high- and low-energy photons are delivered by the low- and high-divergence part of the beam, respectively. This is expected for a near-diffraction-limited beam and is in agreement with the previous studies [12].

3.3. Effect of the gas pressure and the gas-jet position

The highest photon flux and photon energy has been achieved by optimizing the backing gas pressure and the position of the jet relative to the focal spot of the laser beam. The measurement was realized with the EDX detector by recording the spectra at several pressures (figure 5(a)) and integrating the counts in the different channels (figure 5(b)). Below 100 mbar, the integrated signal shows a quadratic dependence on the pressure, implying phase matching [19]. At 100 mbar, the spectrum extends beyond 0.6 keV and has its maximum at about 0.3 keV. The signal below $\sim$200 eV is suppressed by the applied Ti and Al filters as well as the He background. A further increase of the pressure results in a cut-off at lower energies and a reduction of the integrated photon number. The observed behaviour is a consequence of the reduced phase matching length

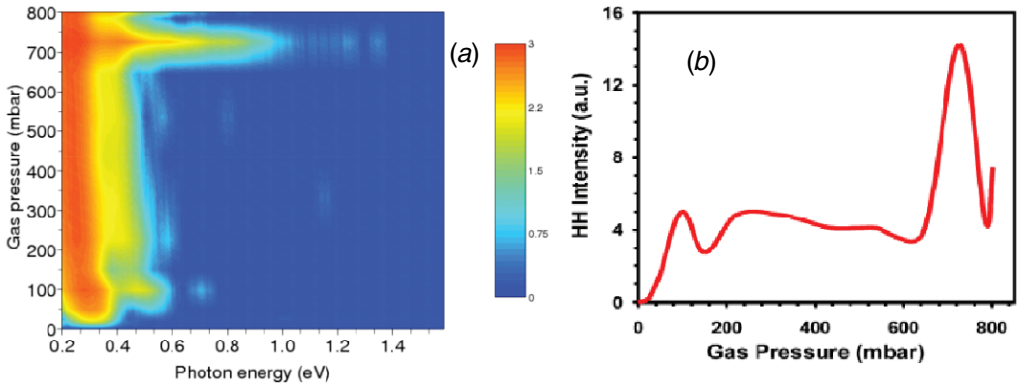

Figure 5. Measured spectra (*a*) for different gas pressures and (*b*) the spectrally integrated photon number at different gas pressures calculated from the data displayed (*a*).

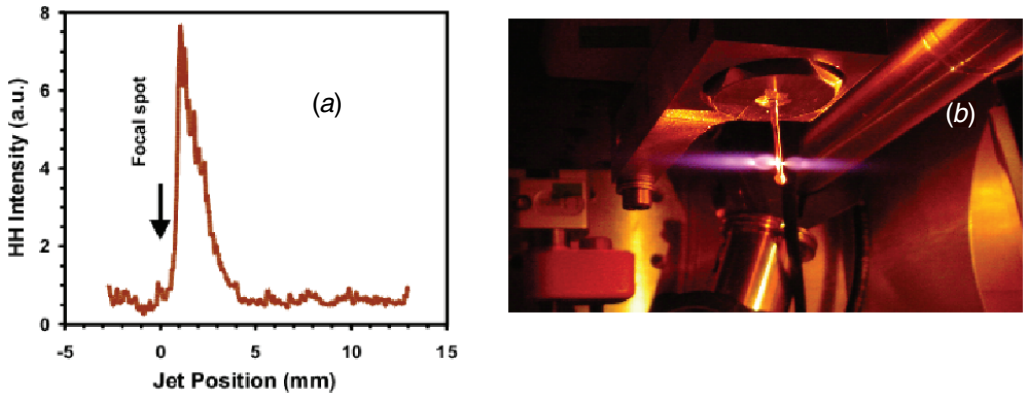

Figure 6. (*a*) Measured HH intensity at different positions of the He gas jet relative to the focal spot of the driving laser beam. (*b*) A photo of the gas jet showing different visible plasma emission in front and behind the gas jet as expected for the asymmetric position to obtain the maximum HH signal.

and the increased re-absorption of the radiation by the higher He background pressure. However, at about 700 mbar, not only the photon number is increased by a factor of four, but also the cutoff is shifted well above 1 keV. The well-pronounced maximum as a function of the pressure backs our assumption of the onset of an additional phase matching contribution in a limited parameter range.

We further optimized the signal by moving the gas jet relative to the focal spot [19]. As seen in figure 6 (a), sharp maximum is observable at a position of 1 mm after the focus. For this optimum position the estimated photon number is an order of magnitude higher compared to the signal obtained with the jet positioned at the focal spot. From the picture in figure 6, taken at the optimum position, it can be clearly seen that the visible plasma emission in front of the gas jet is much stronger than on the backside implying higher laser intensity there. By putting the jet into the focus the emission on both sides become comparable. The maximum signal for the jet out of focus is a clear indication for HH generation and rules out incoherent plasma radiation, where the maximum signal is expected for a gas jet in the focus.

4. Theoretical consideration of HHG in helium

In order to analyse our experiments, we adopted a semiclassical model, based on [20]–[22]. In this model, the single-atom dipole response is calculated by adding contributions from different trajectories, each of which is a product of three terms:

$$\mathrm{d}(t) = \mathrm{Re}\left[\sum_{t_\mathrm{b}} \frac{1}{\sqrt{i}} a_\mathrm{ion}(t_\mathrm{b}) a_\mathrm{pr}(t_\mathrm{b}, t) a_\mathrm{rec}(t)\right], \tag{3}$$

where a_ion is responsible for ionization, a_pr accounts for propagation of the electronic wavepacket in the continuum, and a_rec is responsible for recombination. Each trajectory begins at a moment t_b, when an electron appears in the continuum, and it ends at a time t, when the electron recollides with its parent ion. For a given recollision time t, the possible birth times are determined by the equation $P(t_\mathrm{b}, t) - A_1(t_\mathrm{b}) = 0$, where

$$A_1(t) = -\int \mathrm{d}t' E_1(t'), \qquad p(t_\mathrm{b}, t) = \frac{1}{t - t_\mathrm{b}} \int \mathrm{d}t' A_1(t') \tag{4}$$

Here $A_1(t)$ is proportional to the vector potential of the laser field (the atomic units are used throughout this section). The 'ionization', 'propagation' and 'recombination' probability amplitudes are given by

$$a_\mathrm{ion}(t_\mathrm{b}) = \sqrt{w(t_\mathrm{b}) n(t_\mathrm{b})}, \tag{5}$$

$$a_\mathrm{pr}(t_\mathrm{b}, t) = \left(\frac{2\pi}{t - t_\mathrm{b}}\right)^{3/2} \frac{(2W_\mathrm{b})^{1/4}}{E_1(t_\mathrm{b})} \exp\left[-\mathrm{i} \int \mathrm{d}t' \left(\tfrac{1}{2}[p(t_\mathrm{b}, t') - A_1(t')]^2 + W_\mathrm{b}\right)\right], \tag{6}$$

$$a_\mathrm{rec}(t) = \frac{p(t_\mathrm{b}, t) - A_1(t)}{\{2W_\mathrm{b} + [p(t_\mathrm{b}, t) - A_1(t)]^2\}^3} \sqrt{n(t)}, \tag{7}$$

where the ionization rate $w(t)$ and the density of neutral atoms $n(t)$ are calculated numerically in the single-active-electron quasi-static approximation [23], W_b stands for the ionization potential and $E_1(t)$is the electric field of the laser pulse. The recombination term $a_\mathrm{rec}(t)$ contains the density of neutral atoms at the recombination moment–the importance of this factor for large depletion rates was pointed out in [24]. Due to this factor the contribution of a trajectory becomes negligibly small, if the ground state is significantly depleted by the moment of recollision. This effect cuts off the high-harmonics generated by neutral atoms long before the $3.2U_\mathrm{p}$ limit, which is illustrated in figure 7.

While our model is based on the single-active electron approximation, which, of course, cannot be applied to double ionization, we can use this model to simulate harmonic response from He^+ ions. In figure 7(a), the ionization probability of a neutral helium atom is compared to the ionization probability of a He^+ ion in the field of a 5 fs, 730 nm Gaussian pulse with the peak intensity of $1.4 \times 10^{16}\,\mathrm{Wcm}^{-2}$. While the concentration of neutral atoms practically drops to zero before the peak intensity is reached, a significant amount of He^+ ions survives and therefore can contribute to the generation of photons [25] up to the $3.2U_\mathrm{p}$ limit, which is equal to 2.3 keV.

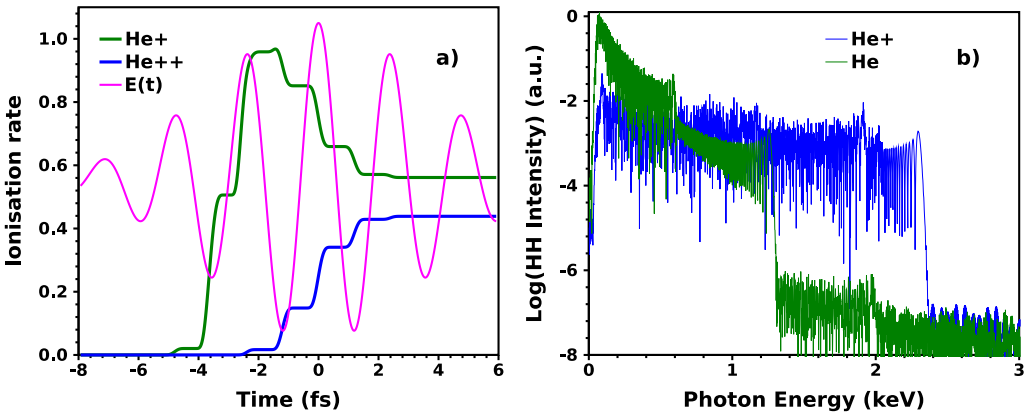

Figure 7. (a) Ionization rate of the He^+ and He^{++} ion in the field of a 5 fs Gaussian laser pulse with the central wavelength of 730 nm and the peak intensity of 1.4×10^{16} Wcm^{-2}. The cut-off photons are generated by the electrons, which are set free near the time -1.2 fs. By this moment, most of He atoms are at least singly ionized. (b) Spectrum of the single-atom/ion dipole response $\partial_t^2\, \mathrm{d}(t)$, which can be considered as the high-harmonic spectrum generated on the beam axis in a very thin target. The green curve shows the contribution of the neutral He atoms calculated in the single-active electron approximation. The blue curve represents the contribution from He^+ ions, which extends up to the $3.2U_p$ limit.

This statement is further supported by figure 7(b), which compares contributions from the single- and the double-ionization channels to the dipole response.

Taking a short comparison between calculation (figure 7(b)) and measurement (figure 3), a major difference can be found. Between 0.5 and 1 keV, the calculation predicts a drop in the yield less than one order of magnitude, contrary to the measurement, where it is about two orders of magnitude. The difference can originate from the not perfectly fulfilled phase matching. The calculation in the recent status is not able to follow the propagation effects. Consequently, the photon yield drops more rapidly than in the calculation and goes under the noise limit of the detector beyond about 1.3 keV. Further improvement of the theoretical model and the laser source would result in higher agreement between the theory and experiment.

5. Summary

We demonstrated a coherent soft-x-ray source driven by 5 fs, 1 mJ laser pulses from a Ti:sapphire amplifier system followed by a hollow-fibre compressor. The generated high-harmonic radiation extends up to photon energies of 1.3 keV and is emitted in a well-collimated beam. For photons centred at 250 eV, the beam has a divergence of $\sim$0.2 mrad. It has also been shown that there exist well-resolved maxima for the cut-off photon energy and the integrated photon number if the He backing pressure or/and the position of the gas jet relative to the focal spot of the driving laser beam are modified. These observations are clear indications for the onset of phase matching.

With the demonstrated x-ray source, it becomes now feasible to extend time-resolved spectroscopy into the several 100 eV range. Due to the increase of x-ray photon number in this

range and by using a waveform controlled few-cycle driver [26], it should be possible to detect single, attosecond x-ray pulses after applying appropriate spectral filtering [7, 8]. Besides shorter pulses the increased cutoff and x-ray flux will open the way to time-resolved x-ray absorption spectroscopy. With an HH-based source the dynamics of chemical reactions or phase transitions can be recorded on a femtosecond time-scale by following the temporal evolution of the x-ray absorption spectra near the absorption edge of a specific atom.

Acknowledgment

This study has been sponsored by the Austrian Science Fund (grants No. F016 P02, P03 and grant No. Z63) and DFG grant SP 687/1-3.

References

[1] Lee T, Jiang Y, Rose-Petruck Ch G and Benesch F 2005 Ultrafast tabletop laser-pump—x-ray probe measurement of solvated $Fe(CN)_6^{4-}$ *J. Chem. Phys.* **122** 084506

[2] Shan F, Carter J D, Ng V and Guo T 2005 Laser-driven hard-x-ray generation based on ultrafast selected energy x-ray absorption spectroscopy measurements of Ni compounds *Phys. Rev.* E **71** 025401(R)

[3] Nishikawa T, Nakano H, Oguri K, Uesugi N, Nakao M, Nishio K and Masuda H 2001 Nanocylinder-array structure greatly increases the soft x-ray intensity generated from femtosecond-laser-produced plasma *Appl. Phys.* B **73** 185

[4] Feurer T, Morak A, Uschmann I, Ziener Ch, Schwoerer H, Reich Ch, Gibbon P, Förster E and Sauerbrey R 2002 Femtosecond silicon K_α pulses from laser-produced plasmas *Phys. Rev.* E **65** 016412

[5] Macklin J J, Kmetek J D and Gordon III C L 1993 High-order harmonic generation using intense femtosecond pulses *Phys. Rev. Lett.* **70** 766

[6] L'Huillier A and Balcou Ph 1993 High-order harmonic generation in rare gases with a 1 ps 1053 nm laser *Phys. Rev. Lett.* **70** 774

[7] Sekikawa T, Kosuge A, Kanai T and Watanabe S 2004 Nonlinear optics in the extreme ultraviolet *Nature* **432** 605

[8] Hentschel M, Kienberger R, Spielmann Ch, Reider G A, Milosevic N, Brabec T, Corkum P, Heinzmann U, Drescher M and Krausz F 2001 Attosecond metrology *Nature* **414** 509

[9] Kienberger R *et al* 2004 Atomic transient recorder *Nature* **427** 817

[10] Paul P M, Toma E S, Breger P, Mullot G, Auge F, Balcou Ph, Muller H G and Agostini P 2001 Observation of a train of attosecond pulses from high harmonic generation *Science* **292** 1689

[11] Tzallas P, Charalambidis D, Papadogiannis N A, Witte K and Tsakiris G D 2003 Direct observation of attosecond light bunching *Nature* **426** 267

[12] Spielmann Ch, Burnett N H, Sartania S, Koppitsch R, Schnürer M, Kan C, Lenzner M, Wobrauschek P, Krausz F 1997 Generation of coherent x-rays in the water window using 5-femtosecond laser pulses *Science* **278** 661

[13] Spielmann Ch, Kan C, Burnett N H, Brabec Th, Geissler M, Scrinzi A, Schnürer M and Krausz F 1998 Near-keV coherent x-ray generation with Sub-10-fs Lasers *IEEE J. Selected Topics Quantum Electron.* **4** 249

[14] Gibson E A *et al* 2003 Coherent Soft x-ray generation in the water window with quasi–phase matching *Science* **302** 95

[15] Seres E, Seres J, Krausz F and Spielmann Ch 2004 Generation of coherent soft-x-ray radiation extending far beyond the titanium L Edge *Phys. Rev. Lett.* **92** 163002

[16] Seres J, Seres E, Verhoef A J, Tempea G, Streli Ch, Wobrauschek P, Yakovlev V, Scrinzi A, Spielmann Ch and Krausz F 2005 Source of coherent kiloelectronvolt s-rays *Nature* **433** 596

[17] Seres J, Verhoef A J, Seres E, Tempea G, Spielmann Ch and Krausz F 2005 A 6 fs sub-terawatt all-solid-state TI: sapphire laser system *Advance Solid State Photonics Conf., Vienna, TuA2*

[18] Tempea G, Geissler M, Schnürer M and Brabec T 2000 Self-phase-matched high-harmonic generation *Phys. Rev. Lett.* **84** 4329

[19] Balcou P *et al* 2002 High-order-harmonic generation: towards laser-induced phase-matching control and relativistic effects *Appl. Phys.* B **74** 509

[20] Lewenstein M, Balcou Ph, Ivanov M Yu, L'Huillier A and Corkum P B 1994 Theory of high-harmonic generation by low-frequency laser field *Phys. Rev.* A **49** 2117

[21] Ivanov M Yu, Brabec Th and Burnett N 1996 Coulomb corrections and polarization effects in high-intensity high-harmonic emission *Phys. Rev.* A **54** 742

[22] Brabec Th and Krausz F 2000 Intense few-cycle laser fields: Frontiers of nonlinear optics *Rev. Mod. Phys.* **72** 545

[23] Scrinzi A 2000 Ionization of multielectron atoms by strong static electric fields *Phys. Rev.* A **61** 041402(R)

[24] Gordon A and Kärtner F X 2005 Scaling of keV HHG photon yield with drive wavelength *Opt. Exp.* **13** 2941

[25] Gibson E A, Paul A, Wagner N, Tobey R, Backus S, Christov I P, Murnane M M and Kapteyn H C 2004 High-order harmonic generation up to 250 eV from highly ionized argon *Phys. Rev. Lett.* **92** 033001

[26] Baltuska A, Udem Th, Uiberacker M, Hentschel M, Goulielmakis E, Gohle Ch, Holzwarth R, Yakovlev V S, Scrinzi A, Hansch T W and Krausz F 2003 Attosecond control of electronic processes by intense light fields *Nature* **421** 611